CFD simulations

Charbel Hage, Tonino Sophy, El-Hassane Aglzim

CFD Analyses of the Aerodynamic Effects on a Quadcopter Propeller in the Proximity of Fixed and Horizontal Moving Obstacles

Charbel Hage[1], Tonino Sophy[1], El-Hassane Aglzim[1]
[1]DRIVE EA1859, Univ. Bourgogne Franche Comté, F58000, Nevers, France
charbel.hage@u-bourgogne.fr, tonino.sophy@u-bourgogne.fr, el-hassane.aglzim@u-bourgogne.fr

Abstract— Quadcopters technology is experiencing strong growth in many fields such as military and civil. They can be used for freight transportation, military surveillance, area maneuvers, and public aerial video and reproduction. When operating around obstacles and in the proximity of walls or moving objects, the aerial vehicle is constrained to many external forces (lift, drag, torque, pitch moment) induced by several aerodynamic effects that can lead to severe flight instability. In this paper, a methodology based on Multiple Reference Frame (MRF) Tetrahedral meshes is developed on a Phantom 3 drone propeller and applied to computational simulations to reproduce the downwash flow generated by the propeller over fixed and moving obstacles. First, a validation of the aerodynamic model is completed, and a convergence mesh study with different rotational speeds (1000-10000 rpm) is performed and validated by comparing it to other experimental data. Then, the effect of fixed or moving obstacle proximity at different horizontal velocities on the phantom 3 propeller performance is assessed and compared to theoretical models. Finally, the simulations results were obtained with velocity fields at different obstacle altitudes (0.1 m, 0.2 m, 0.5 m, 1 m) and different obstacle horizontal velocities (5 m/s, 10 m/s, 15 m/s, 20 m/s) to describe the aerodynamic interference effect of a moving obstacle on the propeller. When hovering at 3000, 5000, and 9550 rpm, the results showed an increase in the lift force on the propeller by 9.3%, and 1.03% comparing to open rotor thrust due to the presence of a fixed obstacle(wall) placed at 0.1 m and 0.2 m from the propeller, respectively. However, when hovering (3000 rpm) at 0.2 m above a moving obstacle (5 m/s, and 10 m/s) the results have shown an increase in the lift by 1.92% for 5 m/s moving obstacle, and then a decrease by 4.4% for 10 m/s, comparing to fixed obstacle thrust. Finally, the horizontal moving obstacle proved to have a significant influence on the aerodynamic performance of the propeller with a decrease in the thrust force at low hovering rotational speed. Indeed, the streamlines in the flow field were coupled to each other in the presence of the moving obstacle with the formation of turbulent vortices and flow separation zones.

Index Terms—UAV, Quadcopter, CFD Simulations, Moving Ground Effect, Thrust Force, Power Loading, Aerodynamic.

I. INTRODUCTION

WITH the huge extension of the UAV technology in logistics and transportation applications such as cargo delivery, surface inspections, and more military applications [1][2][3], several studies are being performed to increase the safety of the UAV flights in urban areas under several specific conditions. The main problem of the small UAVs' flight operation is that they are heavily affected by bad weather, strong wind, and air turbulence because of their small size, slow cruising speed, and low endurance [4]. Also, the external airflow and the disturbances caused by the interference between the downwash flow of the quadcopter propeller and other fixed and moving vehicles have a significant impact on the stability and the aerodynamic performance of the UAV. Therefore, it is very important to study the aerodynamic characteristics of the quadcopter propeller in the presence of a fixed and a moving obstacle. In addition, when the obstacle (wall, car, bus, or a train) is introduced, the incoming airflow generated by the horizontal movement will interfere with the aerodynamic characteristics of the downwash generated by the quadcopter propeller, making the flow field more complicated, affecting the reliability and the stability of the quadcopter UAV.

At this point, the last theoretical and numerical CFD models developed to study the ground effect on the thrust of a sole propeller are not focused on the effect of moving walls and obstacles. Several experimental investigations were carried out to study the effect of the rotation, the position of the rotors, the geometry of the blade, and the effect of a fixed ground on the thrust [5][6]. The results from a sole quadcopter propeller were validated and show good agreement with the theoretical models developed by Cheeseman and Bennett [7]. The ground effect is noticeable at about H/R<2 (H is the ground height and R is the propeller radius) for a sole propeller and at about H/R<4 for a quadcopter [7]. More complex theoretical models based on the Cheeseman and Bennett model were developed and compared to experimental results to predict the fixed ground effect on the quadcopter performance [8][9][10][11][12][13]. Regarding the study methodologies, the evaluation of the aerodynamic performances of quadcopter UAVs when flying near an obstacle is the main concern and a challenging task due to the number of variables concerned in the study. For example, the wind tunnel test has been used with other methods to study the flow generated from the propellers, the ground effect of the induced velocity, and the thrust of the UAV [14][15][16]. Besides, 2D and 3D numerical analyses were performed using CFD computational methods and several approaches have been used to predict the downwash flow of the quadcopter [17][18][19], but none of them reproduces the 3D flow generated by the propellers in the presence of a moving obstacle at several altitude and velocities from the UAV. In this line, the objective of the present paper is to reproduce and evaluate the interaction of the Phantom DJI drone propeller with a fixed and moving obstacle during the hovering flight by CFD simulations. That is, how the presence of a moving obstacle (car, bus, train) in the proximity of the propeller affects the fluid flow around the vehicles and the repercussion on the thrust force and moment parameters of the propeller. This situation is very common specifically in the Deliv'Air project, which is funded by the Bourgogne Franche-Comté region (Région BFC), and consists of operating delivery drones capable of using the existing public transport to ensure rapid and autonomous delivery flight. During the approach, landing, and taking off phases, the UAV might encounter regions with extreme turbulence and fluid separation zones, which could lead to instabilities in the control or to the necessity of variations in the rotors settings.

Thereby, this contribution is split into four sections. After this introduction contained in section I, the geometrical model of

the phantom DJI 3 propeller, the partition of the fluid field, the used mesh grids with the computational methodologies and the boundary conditions of every completed simulation are presented in section II. Next, the validation of the rotation methodology with comparison to experiment data is detailed in section III. Then, the main results of the study are shown and discussed in section IV. Finally, the conclusions of the research are summarized in section V.

II. Materials and Methods

A. Geometrical Model

The propeller of the Phantom DJI 3 standard has been used in this study since it is one of the most sold small quadcopters on the market. This UAV consists of four rotors (diameter of 240 mm) and contains a camera, its mounting assembly, and two support legs (Figure 1).

The front, the side view, and the shape characteristics of the propeller 3D model are described in Figure 2 and Figure 3, respectively.

Figure 1: DJI Phantom 3 original geometry

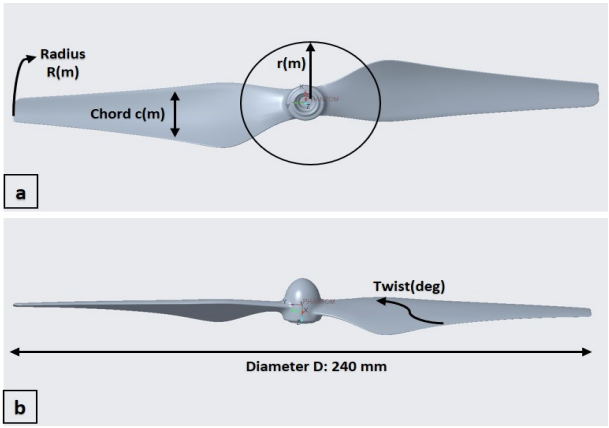

Figure 2: DJI Phantom 3 propeller: (a) Front view, (b) Side View.

The graph in Figure 3 shows the width of the chord and the twist angle of the blade along the radius (from the center to the tip), which agree with the profile of the original geometry.

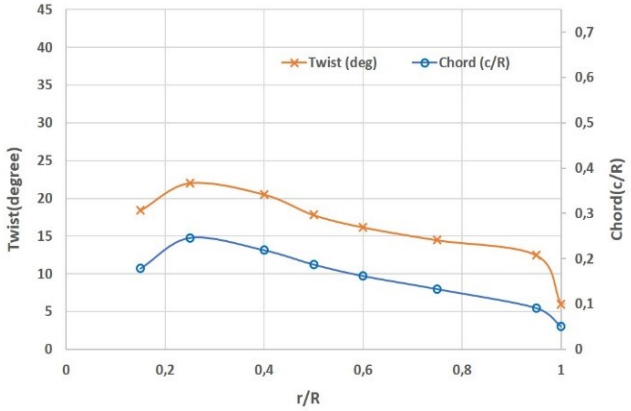

Figure 3: DJI Phantom 3 propeller characteristics

B. Numerical Methodology and Boundary Conditions

In this study, two simulation settings have been used to evaluate separately each of the elements involved in the interaction between a propeller and a fixed or moving obstacle. These two settings (a and b) are summarized in Figure 4 and explained throughout in this section.

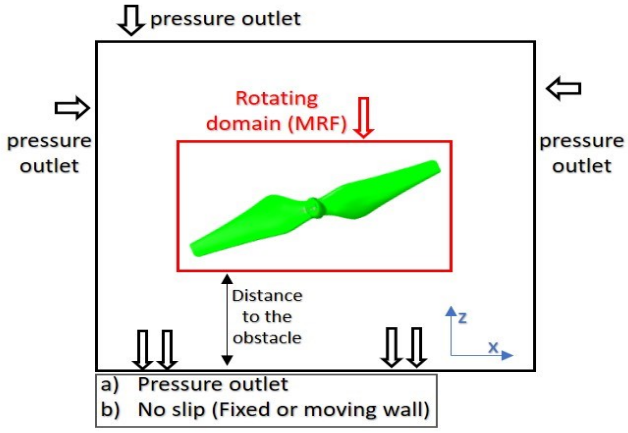

Figure 4: Scheme of different simulation settings used in this study

The case corresponding to Figure 4(a), is used for the characterization of the flow generated by the rotation of the propeller, which is one of the main concerns in the simulation of the flight of a quadcopter, and compare the generated forces with referenced experimental data [5]. Besides, a study of mesh convergence was carried out at different rotor speeds for selecting the optimal meshing parameters. Regarding the rotational method, the Moving Reference Frame (MRF) has been selected and applied to reproduce the rotation of the propeller [20]. This method was applied to the region of fluid directly adjacent to the propeller, enclosed in the cylindrical region named as “rotating domain”. The trustability of the method has been tested against experimental data by estimating the forces exerted by the propeller at different rotational velocities, and the results are shown in section III.

The case corresponding to Figure 4(b), is used to study the effect of obstacle proximity on propeller performance. The distance from the propeller to the obstacle was progressively reduced from 1 m to 0.1 m. Besides, the effect of the fixed obstacle was evaluated at different rotational velocities and different obstacle heights. However, the effect of the moving obstacle on the propeller was studied at 0.2 m height from the obstacle with different moving velocities, and the rotational

velocity was set at 3000 rpm.

C. *Partition of the Fluid Field and Meshes*

As shown in Figure 2, the geometry includes the phantom DJI 3 propeller with a diameter of 240 mm. The simulated fluid domain does not include the propeller part. The total domain was split into the rotational zone, the refining zone around it, and the entire fluid field. The propeller wall, the rotating domain and its dimensions are illustrated in Figure 6. Given the propeller's maximum diameter of D, considering the size of space to be simulated, the total wind field was set to be a rectangular domain with a length of 12.5 x D, a height of 5 x D, and a width of 8.3 x D.

The fluid field was partitioned using design modeler in ANSYS software, and the meshes were generated using ANSYS CFD meshing. As shown in Figure 5 and Figure 6, the boundary conditions of the walls surrounding the outer domain were associated with the outlet, and the no-slip wall corresponded to the methodology used.

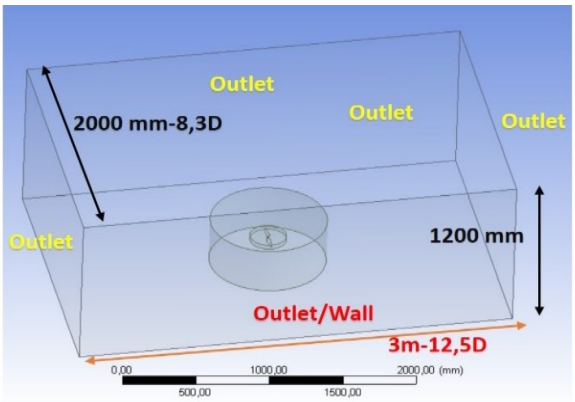

Figure 5: Total fluid partitioning

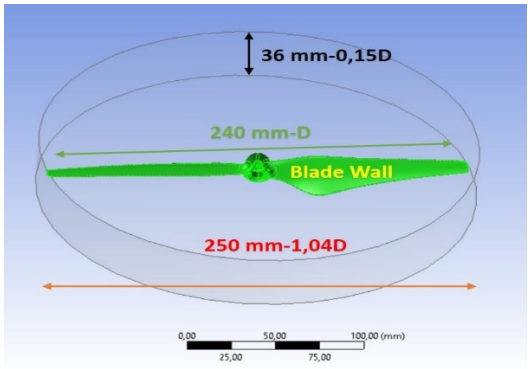

Figure 6: Rotation fluid domain

Considering the efficiency and the fact that the relative dimensions of the propeller were small, an unstructured tetrahedral element was adopted. The resultant meshes are shown in Figure 7, the total number of nodes was 1128087, and the total number of elements was 6433285.

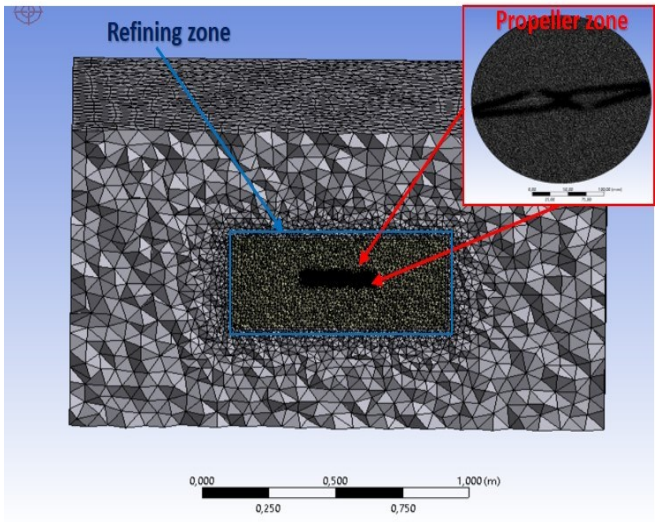

Figure 7: Elements of the entire, refining, and propeller fluid domains

D. *SST Turbulence Model*

The conservation of mass and momentum equations are used in this study to resolve the fluid dynamics problem, and are presented in the equations $\partial\rho\partial t+\left(\rho u_j\right)_j = 0$ (1) and $\frac{\partial \rho u_i}{\partial t} + \left(\rho u_i u_j + p\delta_{ij}\right)_j = \rho f_i + \tau_{ij,j}$ (2).

$$\frac{\partial \rho}{\partial t} + \left(\rho u_j\right)_j = 0 \qquad (1)$$

$$\frac{\partial \rho u_i}{\partial t} + \left(\rho u_i u_j + p\delta_{ij}\right)_j = \rho f_i + \tau_{ij,j} \qquad (2)$$

ρ is the density of the fluid, u the velocity of the fluid, p the pressure of the fluid, τ_{ij} the viscous stress, f_i is a vector representing external forces in i direction, and t corresponds to time [21]. Besides, the later conservation equations are averaged and the Reynolds-Averaged Navier-Stokes turbulent models (K- ω and K- ε) are implemented [22]. These closure equations are primarily used to predict and describe turbulent flows due to the advantages that these models have at low-cost simulations. The k–ε model can reliably simulate the fully developed flow of turbulence far from the wall, while the k–ω model is widely adopted in solving problems for boundary layers in different pressure gradients. Combining the k- ε and the k- ω models, the k- ω shear stress transport (SST) turbulence model has proven its ability to predict flow separation near the wall to reproduce results nearly similar to the experimental ones compared to other turbulence model [23]. Hence, the k- ω SST model was used in this study to simulate the downwash flow of the propeller.

All the simulations were performed in a parallel way in a machine of CPU's with Intel(R) Xeon(R) Silver 4214 with 2.40 GHz processor and 128 gigabytes of RAM. The commercial software ANSYS 22.2 was employed and all the methodologies were calculated in a steady state.

III. Propeller Rotation Methodology

To validate the rotation methodology specified in this paper for the reproduction of the propeller rotation, several simulations have been carried out to reproduce the

experiments published by Deters and Kleinke [5]. The experimental methodology consisted of an isolated Phantom DJI propeller driven by an electric motor mounted in a balance that measures the thrust and the torque. The propeller was tested at different rotational velocities and the results were shown using the thrust and power coefficient expressed by:

$$C_T = \frac{T}{\rho n^2 D^4} \qquad (3)$$

$$C_P = \frac{P}{\rho n^3 D^5} \qquad (4)$$

Where T is the thrust force, P is the power based on the torque Q, ρ is the fluid density, n is the rotational velocity, and D is the propeller diameter.

Concerning the simulations, the phantom DJI 3 propeller was evaluated at six different rpm within the range of the experiments as shown in Figure 8. The C_T, and C_P CFD results of the simulations are dotted in red Diamond and green Plus sign, respectively. The results show good agreement with the experiment data by Deters and Kleinke [5] and with the CFD results by Paz et al [24].

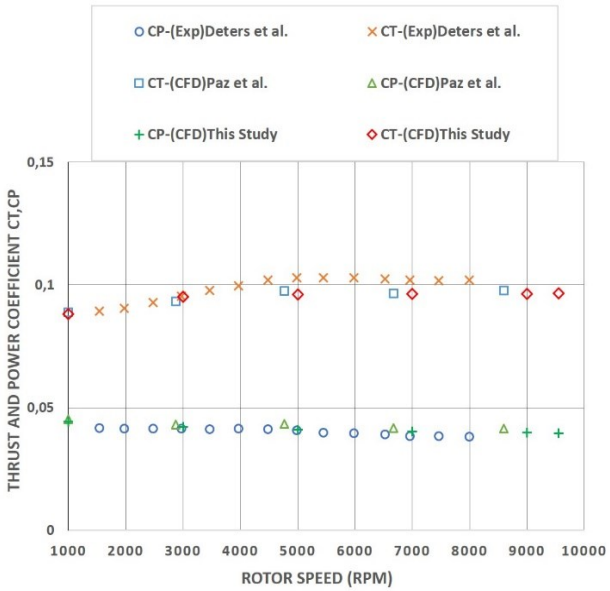

Figure 8: Validation of the rotation propeller methodology

The CFD results of this paper underestimate the thrust coefficient for rotation velocity higher than 3000 rpm. However, this underestimation is inferior to 8 %. Therefore, the rotation methodology used in this study is considered suitable to reproduce the reaction force tested by the propeller due to the generation of the airflow.

IV. Results and Discussion

A. Fixed obstacle effect on the propeller

After the validation, the effect of obstacle proximity on the propeller was studied. For this, several simulations were performed, introducing a solid wall under the propeller at different distances. The boundary conditions have been maintained and the simulations were performed for different rotational velocities (3000, 5000, and 9550 rpm).

Besides, the simulations of the three rotational velocities have been compared to the mathematical model based on the method of images presented by Cheeseman and Bennett [7]:

$$\frac{T}{T_\infty} = \frac{1}{1-\left(\frac{R}{4z}\right)^2} \qquad (5)$$

where R is the propeller radius, z is the vertical distance from the obstacle, T is the thrust generated by the propeller under the effect of the obstacle, and T_∞ is the thrust generated by the propeller in absence of the obstacle. The three velocities cases used in the simulations allows for the consideration of the CFD methodology and the theoretical model to be valid at any rotational speed.

The results are shown in Figure 9, where the thrust force increase is graphed at different height from the obstacle and for different rpm. The thrust force increase percentage is calculated using this formula $\frac{T-T_\infty}{T_\infty}$.

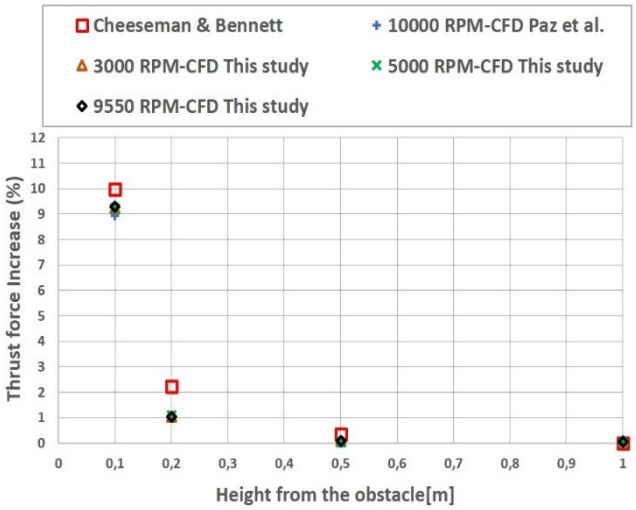

Figure 9: Effect of the obstacle proximity on the propeller

The results from the theoretical model of Cheeseman and Bennett are dotted in red square. Besides, the CFD simulations of this study, the CFD simulations of Paz et al., and the theoretical data follow the same curve, but both CFD results underestimate around 1% of the thrust generated by the propeller at 0.1 m and 0.2 m from the obstacle.

In addition, the velocity fields of the rotor (3000 rpm) in absence of the obstacle is shown in Figure 10. The fluid tube developed by the propeller faces no ground and flows free downwards with a symmetrical and rectilinear trajectory. The reason of the propeller thrust increase at 0.1 m and 0.2 m from the obstacle is illustrated in Figure 11 and Figure 12. The obstacle in close proximity to the propeller forces the flow tube to radially deviate, changing the direction of the flow and causing an increase in the thrust.

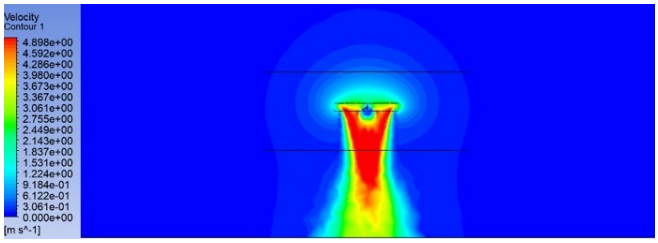

Figure 10: Velocity field, no ground effect, 3000 rpm

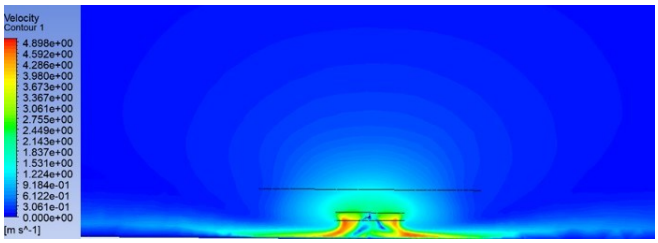

Figure 11: Velocity field, 0.1 m obstacle height, 3000 rpm

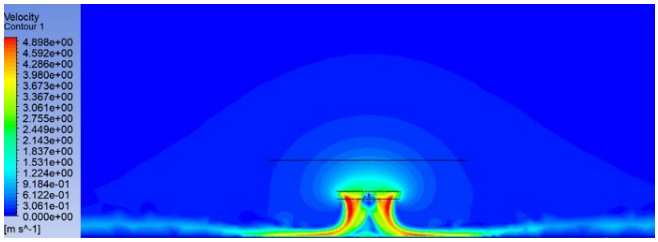

Figure 12: Velocity field, 0.2 m obstacle height, 3000 rpm

As the obstacle moves away from the propeller, the flow is not affected by the wall below and not deviated as shown in Figure 13 and Figure 14.

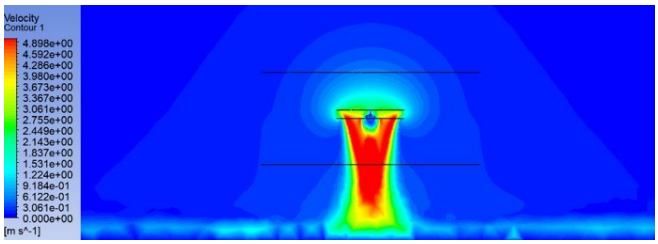

Figure 13: Velocity field, 0.5 m obstacle height, 3000 rpm

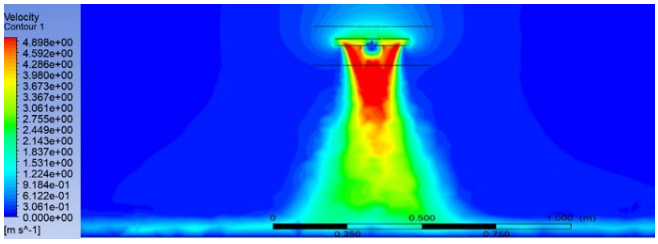

Figure 14: Velocity field, 1 m obstacle height, 3000 rpm

B. Moving obstacle effect on the propeller at 0.2m height

The last step of this study was the evaluation of the moving obstacle effect on the propeller hovering at 3000 rpm at 0.2 m from the obstacle, as it happens when the drone is hovering at a certain altitude waiting for a moving vehicle to approach. This specific study considers only the hovering phase above the moving obstacle and not the approaching or the leaving part of it. The CFD simulations have been performed considering two horizontal velocities of the obstacle and the fixed obstacle case was taken as a comparison reference (1% thrust effect on the propeller). The thrust force variation on the propeller is shown in Figure 15. The results shown an increase in the lift by 1.92% for 5 m/s moving obstacle and then a decrease by 4.4% for 10 m/s comparing to fixed obstacle thrust.

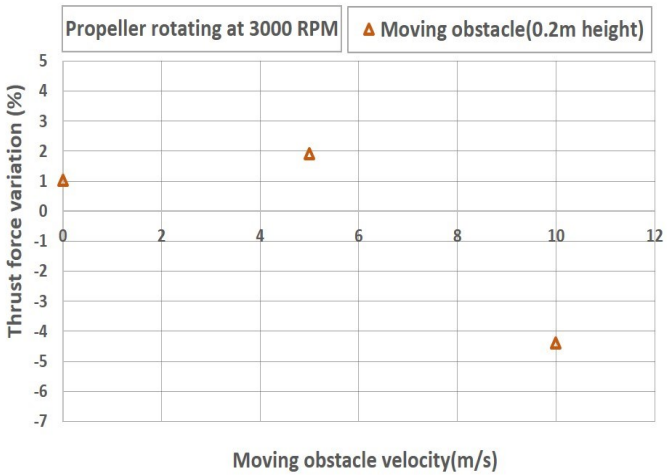

Figure 15: Effect of moving obstacle proximity on the propeller

The reason of the variation in the thrust near a moving obstacle is depicted in Figure 16 and Figure 17, where the velocity fields of the simulations are presented in details. Figure 16 shows the flow over the obstacle moving along (x) direction at 5 m/s, and the downwash of the propeller generated at 4 m/s in both directions (x) and (-x). The flows interfere with each other on the left side of the downwash and a small separation zone appears far from the propeller causing the thrust to increase.

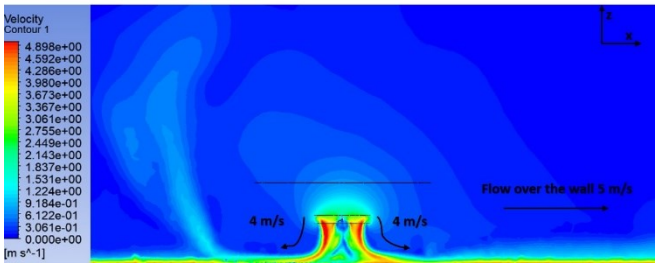

Figure 16: Velocity field, moving obstacle at 5 m/s along (-x) direction

Figure 17 shows the flow over the obstacle moving along (x) direction at 10 m/s, and the downwash of the propeller generated at 4 m/s in both directions (x) and (-x). The flows slightly interfere with each other on the left side of the downwash and a huge separation zone appears next to the propeller causing the thrust to significantly decrease by 4.4%.

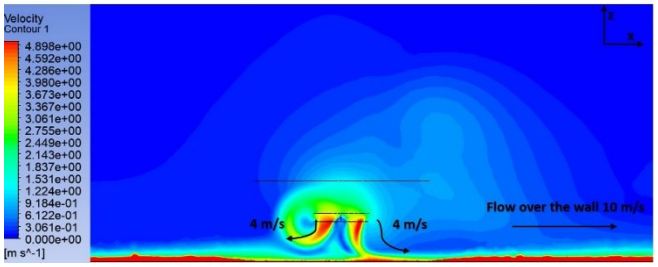

Figure 17: Velocity field, moving obstacle at 10 m/s along (-x) direction

V. CONCLUSION

This paper presented the aerodynamic performance of a Phantom DJI propeller considering the effect of fixed and moving obstacles by numerical simulations. The simulations performed in this study showed to be efficient, indicating a good reproduction of the flow generated by the propeller near moving obstacles at a reasonable computational cost and

avoiding the expenses associated with the experimentation.

As the velocity of the obstacle increases, the swirling flow, and the turbulence dominate the flow field, causing variation in the thrust force on the propeller. This sudden variation on the propeller might cause destabilizations that could even lead to a drop in the vehicle position and a crash with the obstacle in case of no proper reaction of the dynamic system.

In this regard, the results of the present paper lead to new concerns, proposing for future work the necessity of analyzing several cases, which would allow for guaranteeing the safety of the UAV at any possible flying near a moving obstacle.

Funding—This research is part of the Deliv'Air project funded by the Bourgogne Franche-Comte region, France (Région BFC).

REFERENCES

[1] Mai, Y.; Zhao, H.; Guo, S. "The Analysis of Image Stabilization Technology Based on Small-UAV Airborne Video". In Proceedings of the 2012 International Conference on Computer Science and Electronics Engineering, Hangzhou, China, 23–25 March 2012.

[2] Hoffmann, G.; Huang, H.; Waslander, S.; Tomlin, C. "Quadrotor Helicopter Flight Dynamics and Control: Theory and Experiment". In Proceedings of the AIAA Guidance, Navigation, & Control Conference and Exhibit, Hilton Head, SC, USA, 20–23 August 2007.

[3] Pounds, P.; Mahony, R.; Corke, P. "Modelling and control of a large quadrotor robot. Control Eng". Pract. 2010, 18, 691–699.

[4] G. Wild, J. Murray, G. Baxter, "exploring civil drone accidents and incidents to help prevent potential air disasters". Aerospace 3 (2016), https://doi.org/10. 3390/aerospace3030022.

[5] Deters, R.W., Kleinke, S., Selig, M.S., 2017. "Static testing of propulsion elements for small multirotor unmanned aerial vehicles". In: Proceedings of the 35th AIAA Applied Aerodynamics Conference. American Institute of Aeronautics and Astronautics.

[6] Bernard, D.D.C., Giurato, M., Riccardi, F., Lovera, M., 2017. "Ground effect analysis for a quadrotor platform". In: Advances in Aerospace Guidance, Navigation and Control. Springer International Publishing, pp. 351–367.

[7] Cheeseman, I.C., Bennett, W.E., 1955. "The Effect of Ground on a Helicopter Rotor in Forward Flight". Aeronautical research council.

[8] Bangura, M., Mahony, R., 2012. "Nonlinear dynamic modeling for high performance control of a quadrotor". In: Proceedings of the Australasian Conference on Robotics Automation. Victoria University, Wellington, NewZealand.

[9] Danjun, L., Yan, Z., Zongying, S., Geng, L., 2015. "Autonomous landing of quadrotor based on ground effect modelling". In: Proceedings of the 34th Chinese Control conference (CCC), pp. 5647–5652.

[10] Sanchez-Cuevas, P., Heredia, G., Ollero, A., 2017. "Characterization of the aerodynamic ground effect and its influence in multirotor control". Int. J. Aerospace Eng. 1–17, 2017.

[11] Gao, S., Franco, C.D., Carter, D., Quinn, D., Bezzo, N., 2019. "Exploiting ground and ceiling effects on autonomous UAV motion planning". In: Proceedings of the International Conference of Unmanned Aircraft Systems (ICUAS), pp. 768–777.

[12] He, X., Leang, K.K., 2020. "Quasi-steady in-ground-effect model for single and multirotor aerial vehicles". AIAA J. 58, 5318–5331.

[13] McKinnon, C.D., Schoellig, A.P., 2020. "Estimating and reacting to forces and torques resulting from common aerodynamic disturbances acting on quadrotors". Robot. Autonom. Syst. 123, 103314.

[14] Schiano, F., Alonso-Mora, J., Rudin, K., Beardsley, P., Siegwart, R., Siciliano, B., 2014. "Towards estimation and correction of wind effects on a quadrotor UAV". In: Proceedings of the IMAV.

[15] Tomic, T., Schmid, K., Lutz, P., Mathers, A., Haddadin, S., 2016. "The flying anemometer: unified estimation of wind velocity from aerodynamic power and wrenches". In: Proceedings of the International Conference on Intelligent Robots and Systems (IROS), pp. 1637–1644.

[16] Smeur, E.J.J., de Croon, G.C.H.E., Chu, Q., 2018. "Cascaded incremental nonlinear dynamic inversion for MAV disturbance rejection". Contr. Eng. Pract. 73, 79–90.

[17] Kang, N., Sun, M., 2000. "Simulated flowfields in near-ground operation of single- and twin-rotor configurations". J. Aircraft 37, 214–220.

[18] Raza, S.A., Sutherland, M., Etele, J., Fusina, G., 2017. "Experimental validation of quadrotor simulation tool for flight within building wakes". Aero. Sci. Technol. 67, 169–180.

[19] Kaya, K., Ozcan, O., 2013. "A numerical investigation on aerodynamic characteristics of an air-cushion vehicle". J. Wind Eng. Ind. Aerod. 120, 70–80.

[20] Kakimpa, B., Hargreaves, D., Owen, J., Martinez-Vazquez, P., Baker, C.J., Sterling, M., Quinn, A., 2010. "CFD modelling of free-flight and auto-rotation of plate type debris". Wind Struct. 13, 169–189.

[21] J.D.Anderson. "Fluid Dynamics". In: (2007). en.wikipedia.org/wiki

[22] Menter F R. Zonal. "Two Equation – Model for aerodynamic flows". In: (1993). AIAA Paper 93–2906, 24th Fluid Dynamics Conference, Orlando, FL.

[23] Rezaeiha, Abdolrahim, Hamid Montazeri, and Bert Blocken. "On the accuracy of turbulence models for CFD simulations of vertical axis wind turbines". Energy 180 (2019): 838-857.

[24] Paz, C., Suarez, E., Gil, C., Baker, C., 2020. "CFD analysis of the aerodynamic effects on the stability of the flight of a quadcopter UAV in the proximity of walls and ground". J. Wind Eng. Ind. Aerod. 206, 104378.